Journal of Materials Chemistry A

Accepted Manuscript

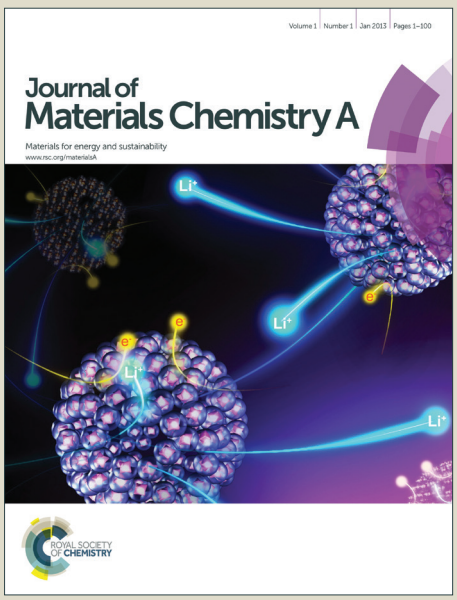

ROYAL SOCIETY OF CHEMISTRY

www.rsc.org/materialsA

Journal of Materials Chemistry A

Cite this: DOI: 10.1039/c0xx00000x

www.rsc.org/xxxxxx

ARTICLE TYPE

A novel synthesis of ultra thin graphene sheets for energy storage applications using malonic acid as a reducing agent

Anil Kumar* and Mahima Khandelwal

Received (in XXX, XXX) Xth XXXXXXXXX 20XX, Accepted Xth XXXXXXXXX 20XX

DOI: 10.1039/b000000x

The present manuscript reports the novel synthesis of ultrathin graphene sheets employing malonic acid as a reducing agent (GRH-MA) under mild pH conditions. AFM reveals their thickness to be 0.41 ± 0.03 nm. XPS of GRH-MA exhibits the increased intensity of C=C band suggesting the effective reduction of graphene oxide (GO) with enhanced sp^2 character. Optical, infrared and Raman spectroscopy, increased C/O ratio in FESEM and TEM analysis also support this observation. Current- voltage (I-V) measurements show about four orders of magnitudes higher conductivity for GRH-MA (4.4 S cm^{-1}) as compared to that of GO (3.05 x 10^{-4} S cm^{-1}). The reduction of GO by oxalic acid (GRH-Ox) under identical experimental conditions was observed to be less efficient as indicated by optical and Raman spectroscopy, and I-V measurements. The efficient reduction by malonic acid is thus understood by the presence of active methylene group, which makes it as an effective nucleophile. XRD of GRH-MA sheets annealed at 300 ^{0}C (GRH-MA300) exhibits the 'd' spacing of 0.35 nm. HRTEM analysis of GRH-MA300 also showed a similar 'd' spacing of 0.35 ± 0.01 nm with hexagonal structure, indicating the formation of more ordered graphitic structure upon annealing. IR analysis of this sample exhibited a significant reduction in the oxygen functionalities and I-V measurement showed more than 4-fold increase in conductivity as compared to that of GRH-MA. In cyclic voltammetry, GRH-MA shows fairly high specific capacitance (C_s) of 173 F/g which is more than 23 fold higher to that of GO (7.5 F/g) at 100 mV/s in 1 M H_2SO_4. Galvanostatic charge-discharge measurements shows the maximum C_s value of 254 F/g at 1 A/g which is more than an order of magnitude higher to that of GO (18.6 F/g) and 1.25 times higher to that of GRH-Ox (202 F/g), respectively. Moreover, 1000 cycles of charge-discharge at 10 A/g exhibits fairly good cyclic stability demonstrating its immense potential for energy storage applications.

Introduction

In recent years, research on ultrathin 2-D graphene sheets has drawn wide attention because of its several attractive optical, electronic, thermal, mechanical, electrical and electrochemical properties. These properties are finding increasing applications in the areas of biological / chemical sensors,[1] transistors,[2] thermal materials,[3] nanoelectromechanical resonators,[4] stretchable transparent electrodes[5] and energy storage materials.[6] A number of approaches have been employed for the synthesis of graphene such as; chemical vapour deposition (CVD),[7] plasma-enhanced CVD,[8] epitaxial growth on electrically insulating surfaces,[9] electric arc discharge[10] and chemical reduction.[11] Among different approaches, chemical method has its own advantages as regards to the high yield, cost effectiveness, mild conditions, ease of synthesis and functionalization. Among different chemical reductants, the reducing agents like hydrazine and its derivative,[12-14] hydroquinone,[15] sodium borohydride,[16] lithium aluminium hydride,[17] urea,[18] hydrohalic acids,[19] sulphur containing compounds[20] and sodium hydrosulfite[21] have been extensively used. Most of these reducing agents, however, are known to be corrosive and toxic.[12-14] Moreover, N-containing reductants often leads to the functionalization of graphene, which reduces its characteristic electronic properties. In recent years, a number of other mild reducing agents containing carboxylic groups such as: oxalic acid,[22-25] tartaric and malic acid[23] have been tried, which are relatively less toxic. Song *et al.*[22] have reported that the reduction of 0.3 mg/mL of graphene oxide (GO) requires 78 mg/mL of oxalic acid and takes 18 h of heating at 75 ^{0}C. The removal of remaining oxalic acid was carried out by further heating of the reaction mixture at 150 ^{0}C for an hour. Teng *et al.*[23] have used 5 mg/mL of oxalic acid, tartaric acid and malic acid for the reduction of 0.5 mg/mL of GO. In this case it needed 24 h of heating at 95 ^{0}C.

Besides the nature of reducing agent the effective reduction of GO to produce graphene requires to explore the effect of different parameters like pH, temperature, concentration of the GO, and

time of reduction under mild conditions. In the present work malonic acid has been employed for the reduction of GO. It required only 6 h of heating at 95 ^{0}C and relatively much lower concentration of malonic acid (1.6 mg/mL) for the complete reduction of GO (0.5 mg/mL). The malonic acid being dibasic acid like oxalic acid, but having an active methylene group, is expected to act as an efficient reducing agent under mild basic pH conditions because of the following possible resonating structures (Fig.1):

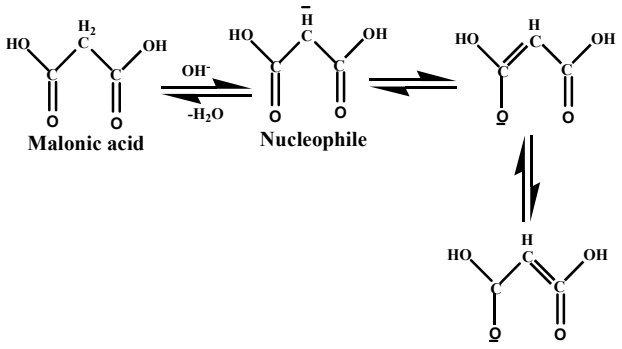

Fig. 1 Resonating structures of malonic acid.

It produced ultrathin sheets of graphene with fairly high conductivity, specific capacitance, charging- discharging capability at high current density and good cyclic stability. Such materials are finding increasing applications as electrode material(s) in energy storage devices.[6]

Experimental section

Chemicals / Materials Used

The chemicals - natural graphite flakes (75+mesh) (Aldrich); malonic acid, hydrochloric acid, hydrogen peroxide (30%), potassium permanganate and phosphorous pentoxide (SD Fine chemicals Ltd.); dimethylformamide (DMF), potassium persulphate (Merck); sulphuric acid (Thomas Baker 98%); oxalic acid (Rankem) and sodium hydroxide pellets (Himedia) procured were of analytical grade and used as received without any further purification. Dialysis tubing (seamless cellulose tubing) along with tubing closures were purchased from Sigma. Fresh millipore water was used for the preparation of solutions.

Equipment

The electronic spectra were recorded on a Shimadzu UV2100 spectrophotometer using 1mm quartz cell. Raman measurements were carried out on an inVia Renishaw spectrometer equipped with 514 nm argon ion laser, CCD detector and a 50X objective lens. X-ray diffraction patterns were recorded on a Bruker AXS D8 Advance X-ray diffractometer (XRD) using Cu Kα line (1.5418 Å) as target at a voltage of 40 kV and having a current of 30 mA. The diffraction patterns were measured in 2θ range of 5 to 40^0 at a scan rate of 0.02^0 per step. NTEGRE (NT-MDT) atomic force microscope (AFM) equipped with NOVA software was used to study the surface topography of the samples by recording 2D images. Digital field emission scanning electron microscope (FE-SEM) QUANTA 200-FEG equipped with energy dispersive x-ray analysis (EDAX) facilities from Oxford instruments and AMETEK materials analysis division with Aztec energy analysis and genesis softwares, respectively. The charged-coupled device (CCD) was employed for the analysis of surface morphologies and performing elemental analysis. Transmission electron micrographs (TEM), high resolution transmission electron microscopy (HRTEM) and selected area electron diffraction (SAED) measurements were obtained on a FEI-TECNAI G^2 20 at an operating voltage of 200 kV. Infrared spectra were recorded in the mid IR range (4000 - 400 cm^{-1}) in KBr medium on a Thermo Nicolet Nexus Fourier transform infrared (FTIR) spectrophotometer and were processed by using OMNIC v6.1 software. X-ray photoelectron spectroscopy (XPS) measurements were performed on an Omicron nanotechnology instrument using Al Kα energy source (1486.6eV). Thermogravimetric analysis (TGA) was carried out in N_2 atmosphere on a SII TG/DTA 6300 EXSTAR at a heating rate of 10 ^{0}C/min in the temperature range of 25- 800 ^{0}C. Zeta potential (ζ) measurements were carried out on a Zetasizer ZS90 (Malvern Instruments) equipped with 632 nm He - Ne laser as a source of light. Current- voltage (I-V) measurements were made on the unit supplied from Photo Emission Tech. Inc., USA equipped with Keithley 2400 source meter and 4200-SCS source meter, respectively at room temperature using four probe method. For these measurements the aluminium electrodes were deposited by using HINDHIVAC 12" vacuum coating unit (Model no. 12A4D). Electrochemical experiments were performed using a CHI760E electrochemical workstation (CH Instruments, USA). The cyclic voltammetry (CV) and galvanostatic charge-discharge (GCD) measurements were carried out using three electrode system employing glassy carbon electrode (GCE 3mm diameter), Ag/AgCl (3M NaCl) and Pt wire as working, reference and counter electrodes, respectively. In all electrochemical measurements, 1 M H_2SO_4 was used as an electrolyte. For performing the reactions at 95 ^{0}C, refrigerated circulating water baths from Lab companion (Model RW- 0525G and 1025G) were used. The pH of the solutions was maintained on a Toshnival digital pH meter (Model CL 54 +). The samples were centrifuged by using REMI microprocessor research compufuge, (Model PR-24). The samples were dried in a vacuum oven procured from Labtech, Daihan Labtech Co. Ltd. The samples were annealed in air using Metrex high temperature furnace equipped with microprocessor temperature controller.

Methodology

For Raman measurements the sample was placed on the clean glass substrate underneath the 50X objective lens and the measurements were carried out in the range of 500- 3500 cm^{-1}. All spectra were measured at low laser power of 1mW in order to avoid the damage of the samples. The calibration was made using silicon reference at 520 cm^{-1}. Samples for AFM analysis were prepared by applying a drop of dilute sample on the glass substrate which was dried at room temperature in the dark. AFM images were recorded in a semi-contact mode by varying the scanning frequency in the range of 1.5 to 3.13 Hz at room temperature. From the AFM images of the sample, the average height along a particular line was measured by using NOVA software. Samples for FESEM analysis were prepared by mounting a small amount of powder sample on the tape and were

then fixed on the aluminium stub. The gold coating was carried out on the surface of these samples to make them conducting. The FE-SEM images were recorded by applying an acceleration voltage of 20 kV. Samples for TEM analysis were prepared by applying a small drop of the dilute sample on a carbon coated copper grid G-200 (size 3.05 mm). The excess sample from the grid was removed by using a tissue paper. The grid was subsequently dried to evaporate the remaining moisture prior to its analysis in dark at room temperature. Electron micrographs of the samples were recorded by scanning the grid at different magnifications under the electron microscope at an accelerating voltage of 200 kV. For I-V measurements, the film was made by applying the drop of liquid sample on transparent conducting indium titanium oxide substrate. Aluminium electrodes were deposited on the as prepared films by using thermal deposition technique under vacuum followed by drying it overnight at 50 ^{0}C. In some cases the contacts were made by using silver paste. The resistivity was calculated by using the below given equation (1):

$$\rho = \left(\frac{\pi t}{\ln 2}\right)\left(\frac{V}{I}\right) \quad (1)$$

Where, ρ is the resistivity (Ω m), t is the thickness of the samples (m), V is the applied potential (V) and I is the current flowing through the material (A). The conductivity (σ) can be calculated using σ = 1/ ρ (S/m). The thickness of the samples was determined to be 4 μm for GO, GRH-MA and GRH-MA300 respectively. Specific capacitance (C_s) (F/g) from CV curves was calculated by using the below given equation (2):

$$\frac{1}{2m \cdot \Delta V \cdot s}\left(\int_{0.8}^{0} idV + \int_{0}^{0.8} idV\right) \quad (2)$$

Where, m is the mass of the material loaded on the electrode (g), ΔV is the change in potential window (V) and s is the scan rate (mV/s), and $\int_{0.8}^{0} idV + \int_{0}^{0.8} idV$ is the total current obtained by the integration of positive and negative sweep in cyclic voltammetry (A). C_s from GCD curves was calculated by using the below given equation (3):

$$C_S = \frac{I \cdot \Delta t}{\Delta V \cdot m} \quad (3)$$

Where, I is the discharge current (A), Δt is the discharging time (s), ΔV is the potential change during discharging step (V) and m is the mass of the active material (g). The powder samples were prepared by drying them in a vacuum oven at 50 ^{0}C for 12 h and were used for the measurements of Raman, XRD, FTIR, XPS and TGA.

Synthesis of GO

GO was synthesized from natural graphite flakes following the modified Hummers method.[26,27] Graphite flakes (1.5 g) were added into the solution containing the preheated mixture of concentrated H_2SO_4 (6 mL), $K_2S_2O_8$ (1.25 g) and P_2O_5 (1.25 g) at 80 ^{0}C. The resulting mixture was stirred at 80 ^{0}C on an oil bath for about 4.5 h followed by its cooling to room temperature. Thereafter, it was diluted with deionised water (DIW) and left overnight. Subsequently, it was filtered and washed repeatedly with DIW using a 2-20 micron filter to remove the residual acid. The product thus obtained was dried overnight under ambient conditions in a vacuum desiccator. The pre-treated graphite flakes were then put into ice cold concentrated H_2SO_4 (60 mL) at 0 ^{0}C. To this solution $KMnO_4$ (7.5 g) was added gradually under stirring by maintaining the temperature below 20 ^{0}C. The resulting mixture was stirred for about 2 h on an oil bath at 35 ^{0}C. It was followed by the addition of 125 mL DIW in an ice bath to keep the temperature at < 50 ^{0}C. The mixture was further stirred for 2 h at 35 ^{0}C, and then additional 350 mL of DIW and 10 mL of 30% H_2O_2 were added into it sequentially. It resulted in a change in color of mixture from greenish black to brilliant yellow. This mixture was left undisturbed for 24 h. Thereafter, it was centrifuged and washed with 10% aqueous HCl (1L) followed by 1L of DIW to remove any remaining acid. The brown product thus obtained was dried at 50 ^{0}C for 24 h. The resulting solid GO was diluted to make its dispersion in DIW (5 mg/mL). GO dispersion was then dialysed for one week to remove the remaining metal species if any.

GO (0.5 mg/mL) dispersion was exfoliated into DIW by sonication under ambient conditions for 30 min. The resulting homogeneous yellow brown dispersion was stable for several months and was employed for performing reduction.

Reduction of GO using malonic acid

The chemical reduction of GO to graphene sheet was carried out using malonic acid as a reducing agent. The ratio of the amount of malonic acid to GO and the time of heating of the reaction mixture were optimized by varying the amount of malonic acid : GO from 1.2 - 5.2 : 1 and 1 to 8 h, respectively. The maximum amount of the product corresponded to malonic acid : GO ratio and time of heating to be 3.2 : 1 and 6 h, respectively and, thereafter, no change in the optical spectra was observed. The completion of the reaction was adjudged by noting a change in the color from yellow-brown to homogenous black. For the optimized sample, 80 mg (1.6 mg/mL or 15.38 mM) of malonic acid was mixed with 50 mL of GO dispersion (0.5 mg/mL) under vigorous stirring and the pH of the resulting solution was maintained at 10.5 by adding dilute NaOH. The resulting reaction mixture was then kept on a water bath at 95 ^{0}C for 6 h. The resultant black suspension was centrifuged and washed with DIW from eight to nine times to remove any residual malonic acid. As synthesised product was then dispersed into DIW at a pH of 10.5 and is denoted as GRH-MA. Annealing of the synthesised GRH-MA was carried out at 300 ^{0}C and has been denoted as GRH-MA300.

In a control experiments the reduction of GO was also carried out by using oxalic acid and OH^- as reducing agent(s) under identical experimental conditions as mentioned above and the resulting product(s) are denoted as GRH-Ox and GRH-OH^-, respectively.

Modification of working electrodes

For the modification of working electrodes, the GCE electrodes were polished sequentially by alumina powder of size 1 μm followed by 0.5 and 0.03 μm using microcloth pad. The electrodes were rinsed in an ultrasonic bath sequentially using

DIW and ethanol for few minutes, respectively. Thus cleaned GCE electrodes were then dried under the flow of N_2. Graphene dispersion was prepared by adding its 1 mg amount into 2 mL DMF (0.5 mg/mL) and 2 μL of this homogeneously prepared sample was dispersed onto the surface of GCE electrode. The electrode surface was then allowed to dry overnight at room temperature. Similar procedure was followed for the preparation of GO and GRH-Ox modified working electrodes. Prior to electrochemical measurements N_2 was bubbled into the electrolyte (1 M H_2SO_4) for 5 min to remove any dissolved oxygen.

Results

Optical studies

The absorption spectrum of GO exhibits a peak and a shoulder at 230 and 302 nm, respectively which can be attributed to π – π* transition due to C=C and n- π* transition corresponding to the C=O group (Fig. 2A-a). The heating of GO (0.5 mg/mL) in the presence of malonic acid (1.6 mg/mL) at pH 10.5 results in a regular change in color from yellowish brown to black associated with a red shift in the absorption peak of GO from 230 to 263 nm after 6 h of reduction (Fig. 2A-b). The time dependent variation in the absorption peak of GO as a function of heating time up to 6 h is shown in Fig. 2B. After 6 h, the reaction mixture shows an absorption band at 263 nm. Thereafter, no shift in the absorption peak was observed (Fig. 2C). It indicates the formation of graphene (GRH-MA) upon reduction of GO by malonic acid due to the restoration of sp^2 character. Digital photographs of GO and GRH-MA obtained upon the reduction of GO are shown in Fig. 2A; Inset. This colloidal dispersion was fairly stable without adding any additional surfactant / stabilizer as was revealed by dynamic light scattering measurement in which the value of ζ-potential was determined to be – 55 mV (Fig. S1, ESI†). It suggests that the malonic acid is acting both as an effective reducing agent as well as stabilizer in the present case.

In a control experiment, the effect of OH^- at the used pH of 10.5 was also analyzed in the absence of malonic acid. The absorption spectra of GRH-OH^- obtained after 6 h of heating is shown in Fig. S2, ESI†. It clearly shows it to be quite different to that obtained in the presence of malonic acid suggesting that OH^- under these conditions does not result in the efficient reduction of GO. It takes much longer period of time for its reduction to take place in OH^-.[27]

Raman analysis

The Raman spectra of graphite, GO, GRH-MA and GRH-MA300 are shown in Fig. 3A and their spectral data are summarized in Table S1, ESI†. The Raman spectra of graphite and GO are very much similar to that reported earlier.[27] An examination of the I_D/I_G ratio for GO and GRH-MA reveals an increase in its value from 0.86 to 0.97 upon heating at 95 ^{0}C for 6 h (Fig. 3A- b and c). This change was further examined as a function of heating time (Fig. 3B), which shows a gradual increase in I_D/I_G ratio as the time of heating increases. The increase in I_D/I_G ratio indicates an enhancement in the graphitic nature in GRH-MA suggesting the restoration of π-conjugated system upon the removal of oxygen functionalities in GO.[28] Raman spectrum due to GRH-MA300 shows an interesting feature, the G band gets red shifted from 1604 to 1596 cm^{-1} in the direction in which sp^2 graphitic character is increased (Fig. 3A- d) as has been reported previously.[29] It suggests that the annealing process leads to the production of more ordered graphitic structure.

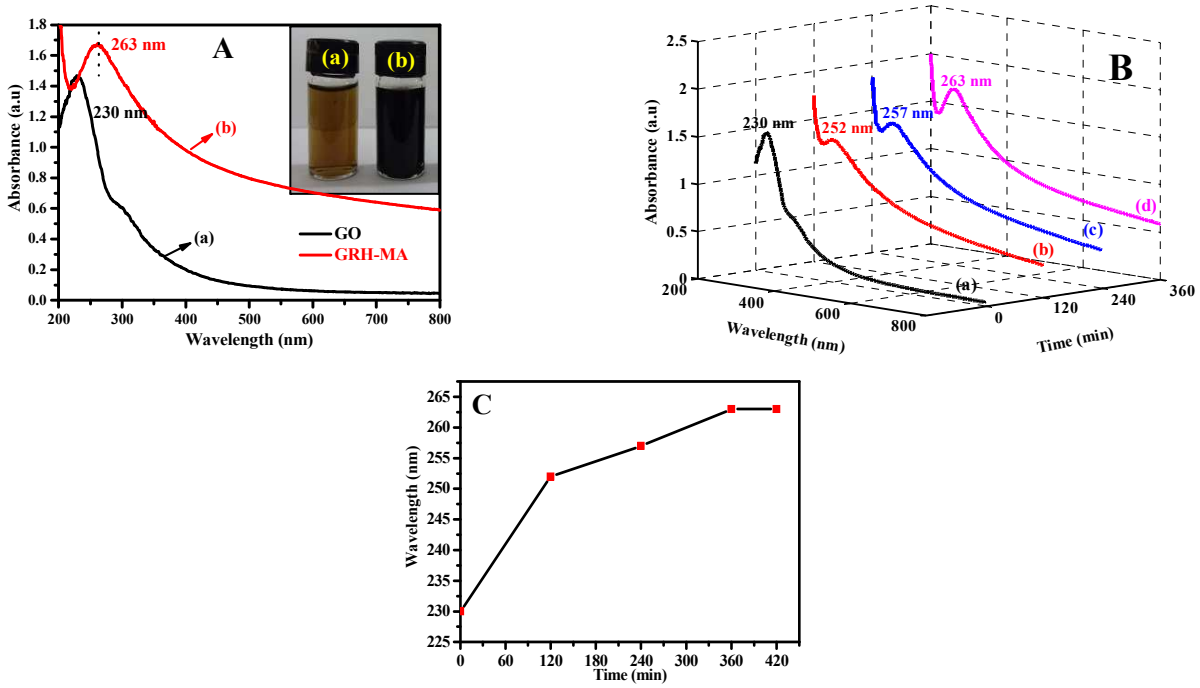

Fig. 2 Optical absorption spectra of GO (a) and GRH-MA (b) - (panel A) along with their digital photographs captured by dispersing them in water – Inset. Changes in the optical absorption spectra of GO as a function of heating time - (panel B). Shift in the absorption maximum of GO with the time of heating - (panel C).

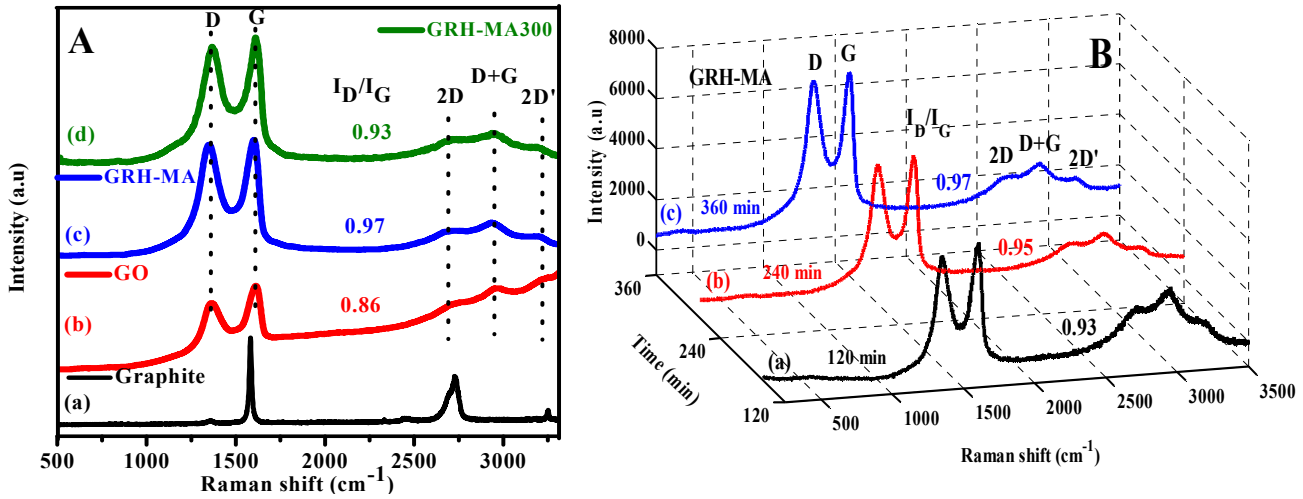

Fig. 3 Raman spectra of: graphite (a), GO (b), GRH-MA (c) and GRH-MA300 (d) – (panel A). Changes in the Raman spectra of GO as a function of heating time – (panel B).

XRD analysis

The XRD patterns of graphite, GO, GRH-MA and GRH-MA300 are shown in Fig. 4. The XRD pattern of graphite exhibits a sharp peak corresponding to (002) plane at 26.2^0 with a 'd' spacing of 0.339 nm, whereas due to GO a slightly broader peak corresponding to the reflection from (002) plane at 10.2^0 with a 'd' spacing of 0.865 nm is observed. These observations are in agreement to the previous report.[27] In contrast to the precursors, graphite and GO, the peak due to GRH-MA is quite broad and is observed at 24.2^0 corresponding to the reflection from plane (002) with a reduced 'd' spacing of 0.36 nm, which is slightly higher than graphite (0.339 nm). To further analyze, the slight difference in the 'd' value of GRH-MA compared to that of pristine graphite, the as synthesised sample was annealed at 300 ^{0}C (GRH-MA300) and the XRD pattern due to this sample shows relatively sharper peak with a reduction in 'd' value of 0.35 nm, which is now closer to that of pristine graphite. The sharpness of peak suggests an increased ordering of the graphene sheet upon annealing for a shorter period of time at mild temperature.[30]

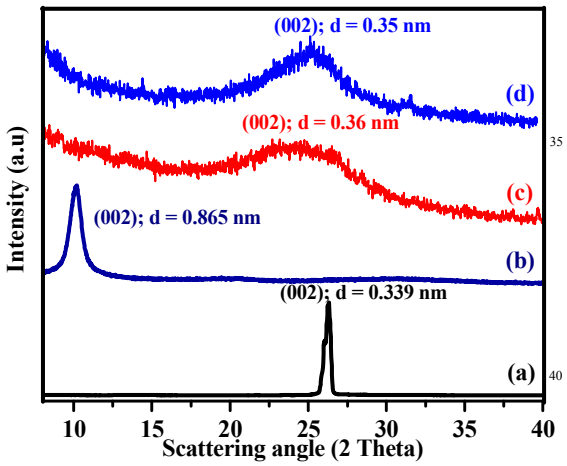

Fig. 4 XRD patterns of graphite (a), GO (b), GRH-MA (c) and GRH-MA300 (d).

AFM analysis

The morphologies of GO and GRH-MA were examined by performing AFM analysis (Fig. 5). AFM images of both the samples show them to contain a sheet like structure. The typical average height of the sheet corresponding to GO and GRH-MA measured along several lines across the respective sheet, gives their thickness to be 1.12 ± 0.1 and 0.41 ± 0.03 nm, respectively. For these samples, the typical images depicting the measurements across a line marked in Fig. 5a and b have been shown in Fig. 5a' and b', respectively. Thus, AFM image of GRH-MA shows it to contain a fairly fine sheet structure, which clearly shows it to be a single layer graphene sheet. It may be mentioned that in previous studies the thickness of the sheet ranging from 0.7 to 1.0 nm has been claimed corresponding to single layer graphene [31-33].

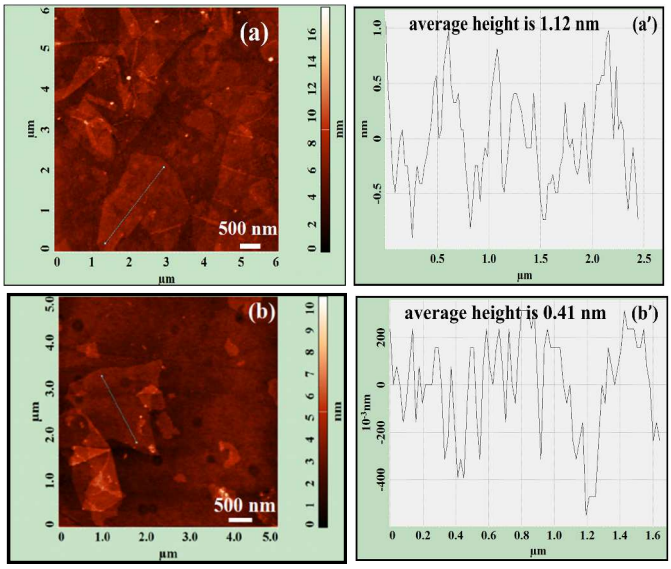

Fig. 5 AFM images and their height profile along a particular line: GO (a, a′) and GRH-MA (b, b′).

FE-SEM analysis

Morphologies of the precursor GO and the products GRH-MA and GRH-MA300 were further examined by recording their FE-SEM images (Fig. 6) and EDAX analysis of these image(s) at the location marked by cross sign in red have been shown below their respective image(s). The FESEM image of GO appears to be agglomerated at different places with a dimension of 95 x 50 µm (Fig. 6a). EDAX analysis of this sheet at the marked location indicate the C/O ratio to be of the order of 1.56 (Fig. 6a′). The FESEM image of GRH-MA shows it to be much finer sheet folded at places (Fig. 6b) with the estimation of its dimension to be 150 x 100 µm. EDAX analysis of this sheet gives C/O ratio of 6.93 which is more than 4 times higher to that of GO indicating the effective reduction of GO (Fig. 6b′ and d). This is also revealed by elemental mapping of the image of this sample recorded at higher magnification (Fig. S3, ESI†), which clearly shows the homogeneous distribution of carbon and oxygen with much higher density of carbon (Fig. 6b″ and b‴).

FESEM image of GRH-MA300 and its line mapping are shown in Figs. 6c and c″. This sheet is extremely thin with fairly high C/O ratio of 9.8 (Figs. 6c′ and d). Thus, a comparison of C/O ratio for these samples exhibit the trend: GRH-MA300 > GRH-MA > GO. Interestingly, annealing of GRH-MA at relatively mild temperature seems to bring increasing removal of some additional oxygen functionalities. It may be pointed out that the employed temperature is much lower compared to those used for the preparation of graphene sheet(s) in which fairly higher temperature were employed.[34]

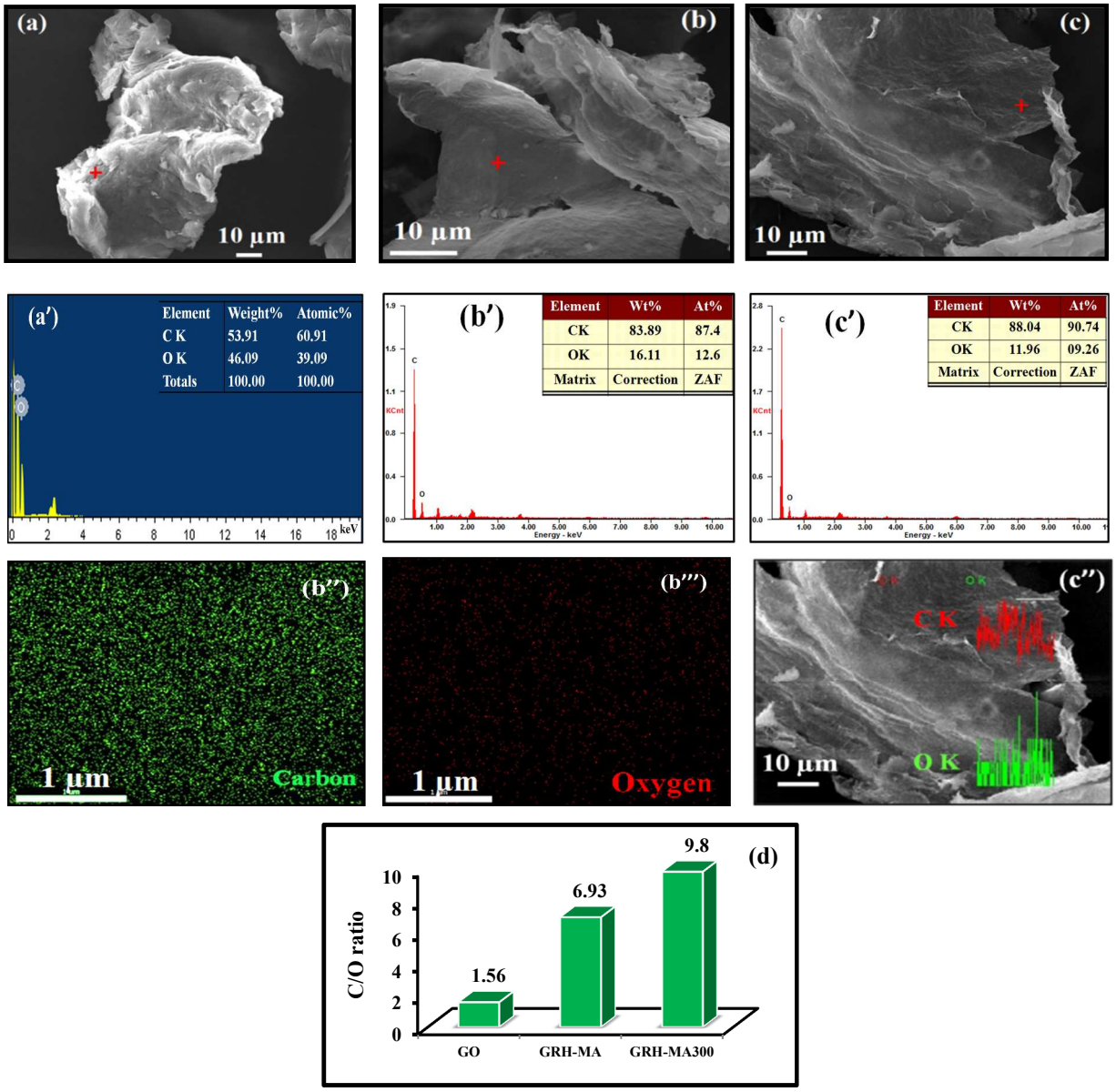

Fig. 6 FE-SEM images and their EDAX analysis on a particular location marked by cross sign in red: GO (a, a′), GRH-MA (b, b′) and GRH-MA 300 (c, c′), respectively; Elemental mapping of GRH-MA: Carbon (b″) and oxygen (b‴). Line mapping of GRH-MA300 (c″). C/O ratio of: GO, GRH-MA and GRH-MA300 (d).

TEM and SAED analysis

TEM images of GO, GRH-MA and GRH-MA300 along with their EDAX spectra and SAED patterns are shown in Fig. 7. TEM image of GO exhibits the formation of sheet like structure. SAED pattern of GO shows it to be polycrystalline and correspond to the planes (101) and (110) of graphite having hexagonal structure matching with the JCPDS file no. 75-1621 (Fig. 7a - Inset). EDAX analysis of this sample shows the C/O ratio to be about 1.40 (Fig. 7a′). On the other hand, the TEM images of GRH-MA and GRH-MA300 shows the formation of very thin sheets (Fig. 7b and c). The SAED pattern of GRH-MA shows the presence of diffused concentric rings indicating its amorphous nature (Inset - Fig.7b). Whereas, in the case of GRH-MA300, it exhibits the formation of crystalline hexagonal structure displaying six fold symmetry (Inset - Fig.7c). Moreover, the electron diffraction pattern of GRH-MA300 exhibits the intensity of inner spots to be much stronger as compared to those of outer spots. The similar SAED pattern has earlier been assigned to monolayer graphene.[35] EDAX analysis of these samples exhibit the C/O ratio to increase in the order GO < GRH-MA < GRH-MA300 (Fig. 7a′, b′ and c′). In the HRTEM image of GRH-MA300 lattice fringes are observed with an average 'd' spacing of 0.35 ± 0.01 nm (Fig. 7c‴), which is in agreement with the XRD results (Fig. 4).

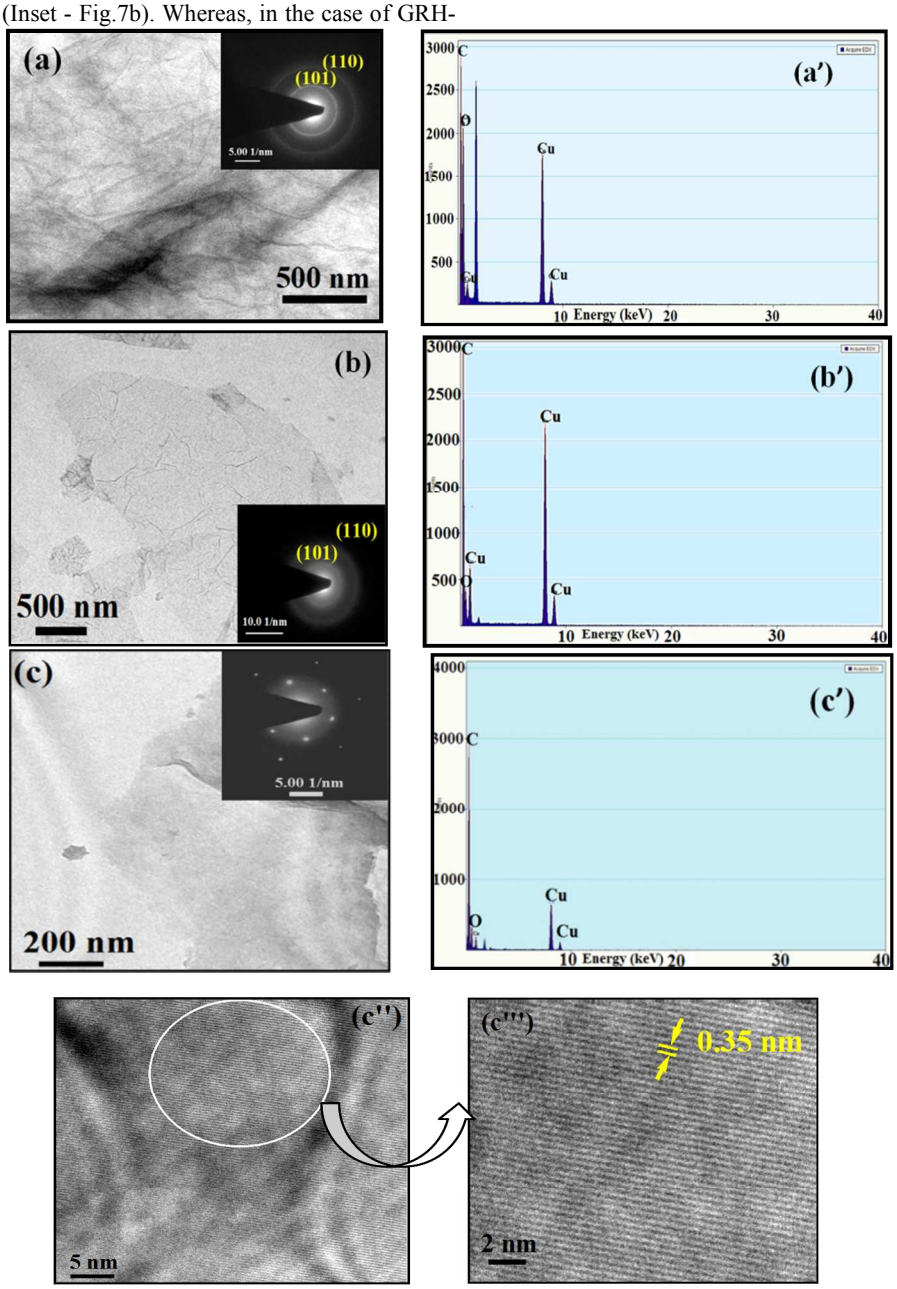

Fig. 7 TEM images along their EDAX analysis and with their SAED patterns in inset of: GO (a, a′), GRH-MA (b, b′) and GRH-MA300 (dispersed in acetonitrile) (c, c′). HRTEM image of GRH-MA300 (c″) and its magnified image (c‴).

IR analysis

IR spectra of GO, GRH-MA and GRH-MA300 in the mid IR range (4000- 500 cm^{-1}) are shown in Fig. 8. The IR spectrum of GO shows fairly intense bands (cm^{-1}) at: 3425, 1718, 1632, 1222 and 1054 which could be assigned to -OH, C=O (–COOH), C=C, C-O-C (epoxy) and C-O (alkoxy), respectively. In the IR spectrum of GRH-MA the intensity of peaks due to –OH stretching (3425 cm^{-1}) and C-O (1054 cm^{-1}) are significantly reduced. The peak due to C=O (1718 cm^{-1}) and C-O-C (1222 cm^{-1}) are completely vanished, whereas the peak due to C=C at 1632 cm^{-1} is still retained in GRH-MA. These observations clearly suggest the sp^2 character is enhanced in reduced GO. The IR spectrum of GRH-MA300 shows further reduction in the intensities of –OH stretching (3425 cm^{-1}) and C-O (1054 cm^{-1}) peaks suggesting the increased elimination of oxygen functionalities of GO.

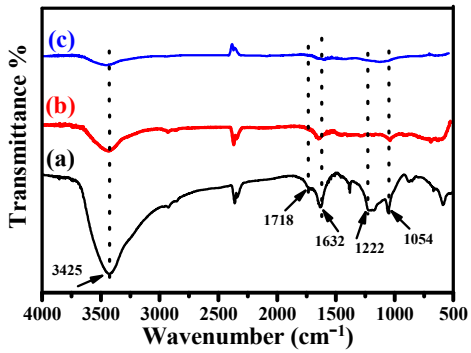

Fig. 8 IR spectra of: GO (a), GRH-MA (b) and GRH-MA300 (c).

XPS analysis

The surface analysis of precursor GO and product GRH-MA was carried out by using XPS in the binding energy range of 200-800 eV (Fig. 9 - panel A). The high resolution C 1s spectrum of GO is shown in panel B. It exhibits four different components of carbon at a binding energy (eV) of: 284.3, 286, 286.8 and 288. These bands could be assigned to C=C (aromatic sp^2 structure), C-C (sp^3 hybridised carbon) / C-OH, C-O (epoxy/ alkoxy) and C=O (carboxylic group), respectively. Whereas, the XPS spectrum of GRH-MA in panel C shows 3 different components of carbon at a binding energy (eV) of: 284.4, 285.6, 288.1 corresponding to C=C (aromatic sp^2 structure), C-C (sp^3 hybridised carbon), C=O (carboxylic group), respectively. A comparison of the C 1s spectra for GO and GRH-MA in panel B and C clearly shows the increased intensity of C=C band at 284.4 eV and the absence of the carbon component at 286.8 eV corresponding to C-O of epoxy/alkoxy for GRH-MA. It suggests that after reduction the relative contribution of carbon species singly bonded and doubly bonded to oxygen is reduced significantly. A comparison of O 1s spectra of GO and GRH-MA (panel D) reveals the elimination of the oxygen functionalities in GRH-MA as was evidenced by a reduction in the intensity of this peak by more than a factor of 7. It thus suggests the effective reduction of GO into GRH-MA exhibiting the enhanced sp^2 character.

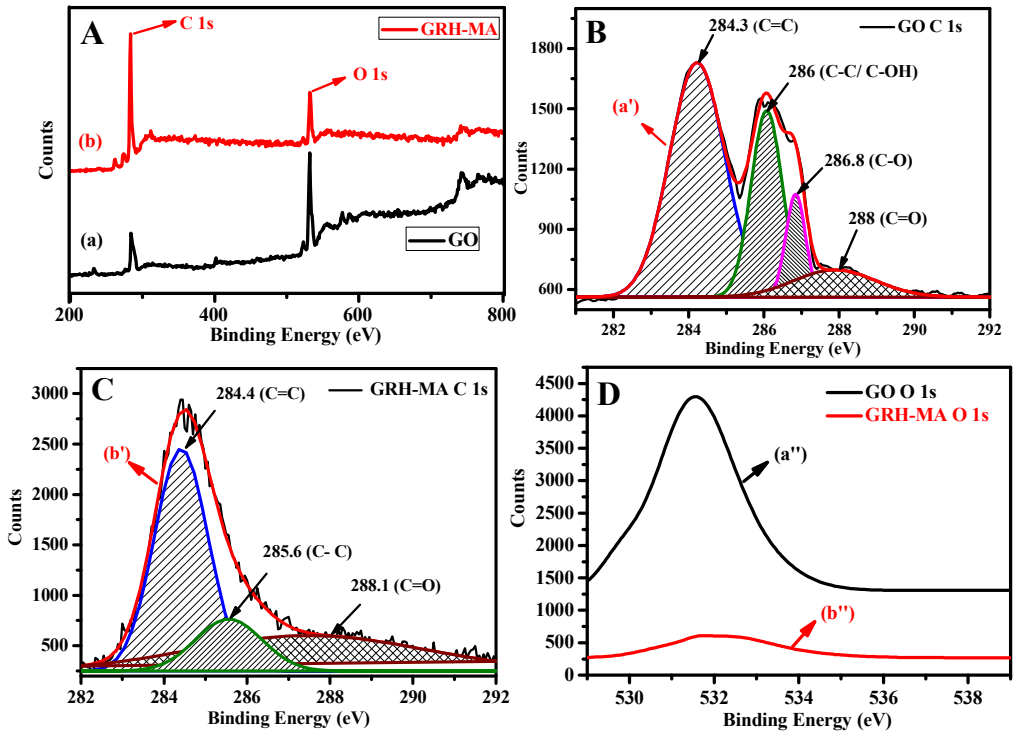

Fig. 9 XPS survey scan of: GO (a) and GRH-MA (b) – (panel A); GO C 1s (a′) – (panel B); GRH-MA C 1s (b′) - (panel C); GO O 1s (a″) and GRH-MA (b″) – (panel D).

TGA analysis

The thermal stability of the precursors graphite, GO and malonic acid along with the reduction products GRH-MA and GRH-MA300 were analysed by TGA (Fig. 10). For graphite the TGA curve was very similar to that reported in literature.[27] For GO, the specific losses were observed in three stages corresponding to the temperatures 115, 215 and 305 ^{0}C accounting for a mass loss (%) of: 19, 59 and 68.6, respectively (curve b). These losses have been attributed to the removal of adsorbed water, the decomposition of labile oxygen functionalities (carboxylic, anhydride and lactone groups) and removal of relatively stable oxygen functionalities (phenols and carbonyl) similar to those observed earlier.[36] However, for the GRH-MA significantly less weight losses (%) of: 15, 23 and 33 were observed at 115, 215 and 305 ^{0}C, respectively (curve d). This sample remains fairly stable beyond 320 ^{0}C up to 1100 ^{0}C (not shown). TGA analysis of GRH-MA300 shows further improved thermal stability in all respect (curve e). In this case the total extent of losses recorded up to 1100^{0}C suggests this sample to have fairly high stability.

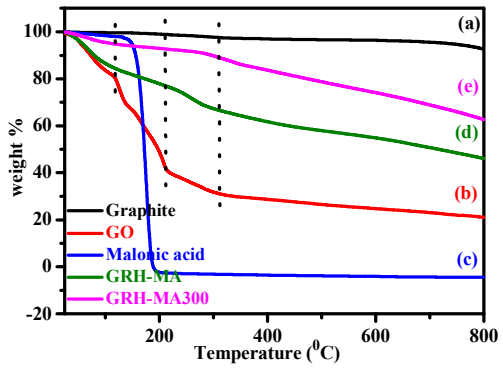

Fig. 10 TGA-DTA curves of graphite (a), GO (b), malonic acid (c) GRH-MA (d) and GRH-MA300 (e).

I-V characterstic

Electrical conductivity was determined by recording the I-V plots for the precursor GO, its reduction products GRH-MA and GRH-MA300 (Fig. 11). A comparison of their I-V curves evidently shows a tremendous increase in the conductivity of GRH-MA (4.4 S cm^{-1}) as compared to GO (3.05 × 10^{-4} S cm^{-1}).

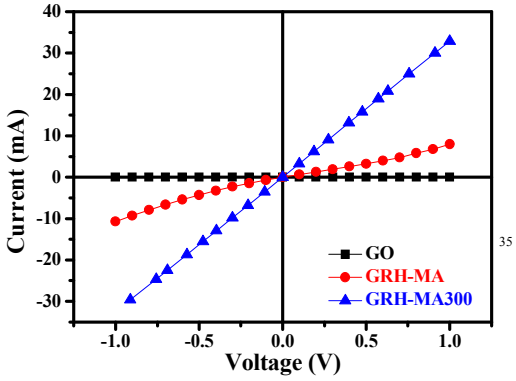

Fig.11 I-V curves of GO (black), GRH-MA (red) and GRH-MA300 (blue).

The 10^4 fold increase in conductivity for GRH-MA as compared to that of GO confirms the restoration of π- conjugation in GRH-MA. The value of conductivity is further enhanced to 18.1 S cm^{-1} in GRH-MA300, which is more than 4 times higher to that of GRH-MA. It is understood by increasing restoration of sp^2 hybridised carbon upon annealing. It may be mentioned that this value of conductivity is even higher to that of graphene paper (obtained by the reduction of GO paper by immersion into HI solution) annealed at 800 ^{0}C.[29]

Electrochemical studies

The electrochemical properties of GRH-MA as electrode material were investigated for energy storage applications. Cyclic voltammograms of GRH-MA recorded at different scan rates ranging from 10 - 100 mV/s in the voltage range of 0 to 0.8 V shows an increase in current response with increasing scan rate (Fig. 12A). From these CV curves the C_s for GRH-MA at scan rates of 10, 30, 50, 70 and 100 mV/s were calculated to be 279, 227, 204, 190 and 173 F/g, respectively (Fig. 12C). For the identical scan rates the value of C_s for GO were observed to be 22, 15, 12, 10 and 7.5 F/g, respectively (Fig. 12B and C). A comparison of CV curves of GRH-MA and GO reveals that at different scan rates, the areas covered under the CV curves for GRH-MA was much higher as compared to that of GO and exhibits typical rectangular shape as compared to that of distorted CV curve for GO (Fig. 12D). For the typical higher scan rate of 100 mV/s, the value of C_s for GRH-MA is 23 fold higher (173 F/g) to that of GO (7.5 F/g), while retaining almost the rectangular shape and also behaving as an efficient electrical double layer capacitor (EDLC), thus suggesting its good capacitive performance (Fig. 12D).

The C_s was also measured by designing the charge-discharge experiments for GRH-MA and GO as electrode materials. Fig. 12E shows the charge-discharge curve for GRH-MA at different current densities: 1 2, 3, 5, 7 and 10 A/g. The shape of the charge-discharge curve is typical symmetrical triangular for all the current densities. For GRH-MA a variation in the current density from 1 to 10 A/g results in the reduction of C_s from 254 to 171 F/g (Fig. 12F). It thus shows that even for the high current density of 10 A/g a fairly higher value of C_s is retained. In a control experiment charge-discharge curve for GO was also recorded at a current density of 1 A/g and it was observed to be 18.6 F/g, which is significantly lower to that of GRH-MA (Fig. 12G).

The long term cycling stability for the highest current density of GRH-MA was further examined by fixing the current density at 10 A/g. From these measurements the C_s for the 1st Cycle was observed to be 171 F/g which increases slightly to 177 F/g after 1000th cycle. A variation in C_s was also examined as a function of the number of cycles (Fig. 12H). For the first 50 cycles, there was virtually no change in the C_s value and, thereafter, it showed a gradual, but fairly small increase in capacitance from 171 F/g to 177 F/g up to 200 cycles and thereafter up to 1000th cycle the C_s value remained virtually unchanged (Fig. 12H- Inset). A small increase noted in the initial 200 cycles might have been contributed due to the removal of small number of residual oxygen functionalities on GRH-MA, as was also indicated by its slightly higher thickness (0.41 ± 0.03 nm) as compared to that of single layer graphene (0.34 nm). Moreover, a partial contribution

to this increase might also be possible due to the wetting of the electrode material.

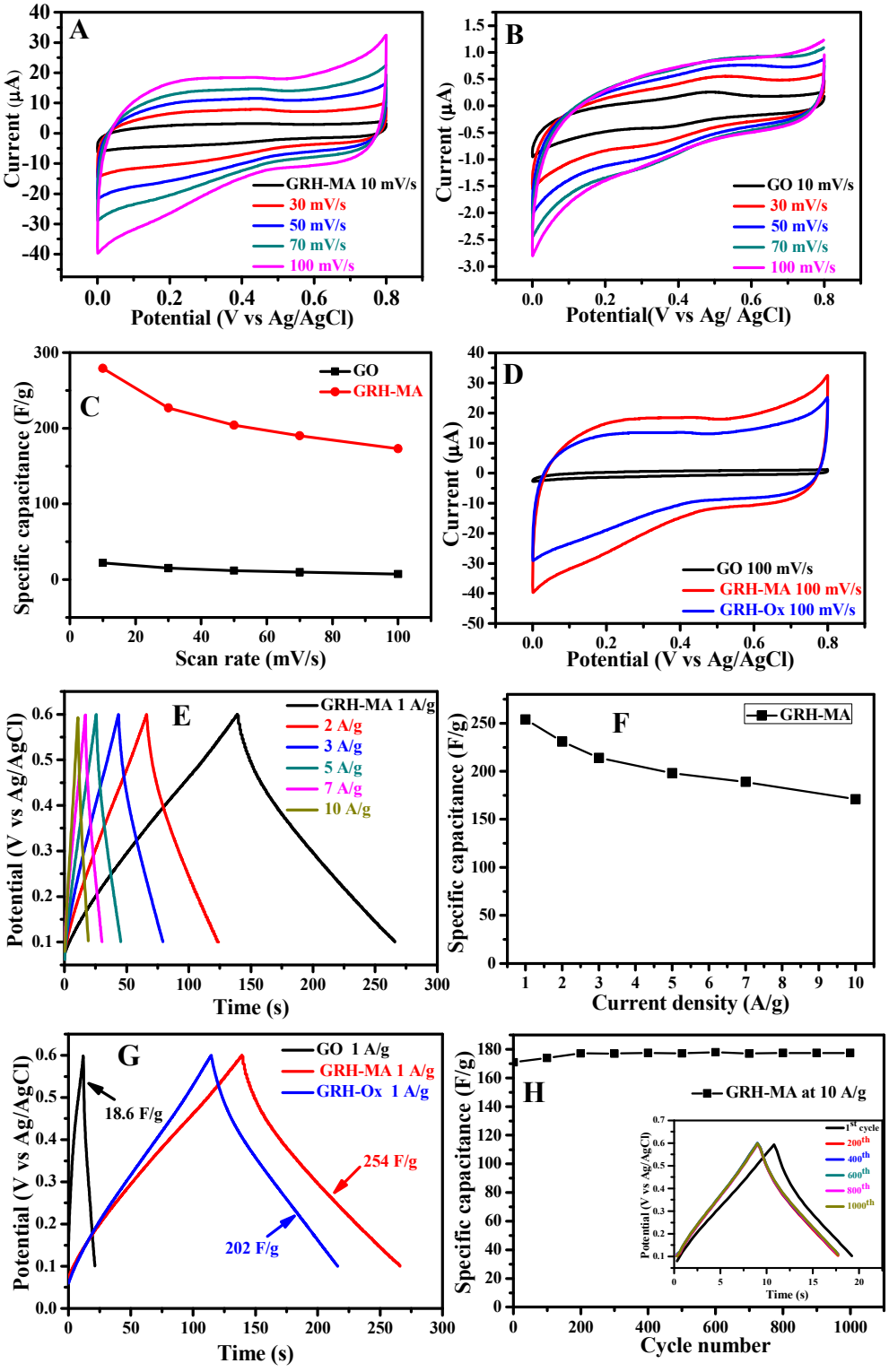

Fig. 12 CV curves of GRH-MA and GO at different scan rates in 1 M H_2SO_4 - (panels A and B). Variation in the value of specific capacitance (C_s) as a function of scan rate for: GO and GRH-MA – (panel C). CV curves of GO, GRH-MA and GRH-Ox at a scan rate of 100 mV/s – (panel D). Galvanostatic charge–discharge (GCD) curves of GRH-MA at different current densities – (panel E). Variation in the C_s value obtained from GCD curves for different current densities – (panel F). GCD curves of GO, GRH-MA and GRH- Ox at a constant current density of 1 A/g – (panel G).Variation in the C_s value as a function of cycle number and their GCD curve in inset - (panel H).

Discussion

It is interesting to observe that malonic acid at mild pH (10.5) results in the effective reduction of GO into graphene as was evident by their optical absorption, Raman spectra, XRD and microscopic techniques (Figs. 2-7). The effective reduction at mild pH is understood by the increased nucleophilicity of stable malonate ion formed under these conditions having active methylene group, which is stabilized by the presence of electron withdrawing carbonyl groups (*vide ut supra*). In view of the pK_a(s) of malonic acid (2.83 and 5.69), at pH 10.5 when both the –COOH groups exist largely as $–COO^-$, one might consider the reduction of GO to be occurring through COO^-. This aspect was further probed in a control experiment by employing oxalic acid, containing two –COOH groups, as a reducing agent under identical conditions of pH, which lacks the presence of active methylene group. The complete reduction of GO by oxalic acid to GRH-Ox takes relatively much longer period of time (9 h), as was evidenced by recording its optical absorption at different times (Fig. S4, ESI†). The fact that oxalic acid has lower pK_a(s) of 1.25 and 4.14 as compared to that of malonic acid, but still is less effective as a nucleophile in mild basic pH conditions (pH 10.5), clearly suggests the participation of active methylene group in malonic acid making it more prominent as nucleophile (Scheme 1). The higher efficiency of reduction of GO by malonic acid is also supported by Raman data in which the I_D/I_G ratio for GRH-MA was found to be 0.97 as compared to that of GRH-Ox in which the I_D/I_G ratio was observed to be 0.95 after complete reduction (Fig. S5, ESI†). The higher I_D/I_G ratio has earlier been suggested due to the restoration of sp^2 carbon upon reduction of GO.[28]

The effect of pH was further investigated by performing the reduction of GO at low pH (6.0) employing malonic acid as reductant. At this pH, the canonical structures for malonic acid are relatively less stabilized and would act as a nucleophile with a limited capability. It was evident by the optical absorption and Raman spectrum obtained upon the reduction of GO after heating for 6 h at 95 ^{0}C (GRL-MA) (Figs. S6 and S7, ESI†). At pH 6.0, I_D/I_G ratio from the Raman spectrum recorded after 6 h of reaction was found to be 0.92, which is less than that observed at pH 10.5 (0.97) during the same period of reaction. It took much longer time for the completion of reduction as was seen by recording their optical and Raman spectrum.[37] It suggests the more effective restoration of graphitic structure of this system at pH 10.5.

An increase in sp^2 restoration of GRH-MA was further indicated by its EDAX analysis using FESEM, which showed more than four times increase in C/O ratio as compared to that of GO (Fig. 6). The disappearance of the peak due to C=O and C-O-C, and retaining of the C=C peak in IR spectroscopy; the absence of C-O of epoxy/alkoxy and increase in the intensity of C=C in XPS evidently suggests the enhanced sp^2 character in GRH-MA. It is also supported by I-V measurements in which about four orders of magnitudes higher conductivity was noted for GRH-MA (4.4 S cm^{-1}) as compared to that of GO (3.05 x 10^{-4} S cm^{-1}) (Fig. 11).

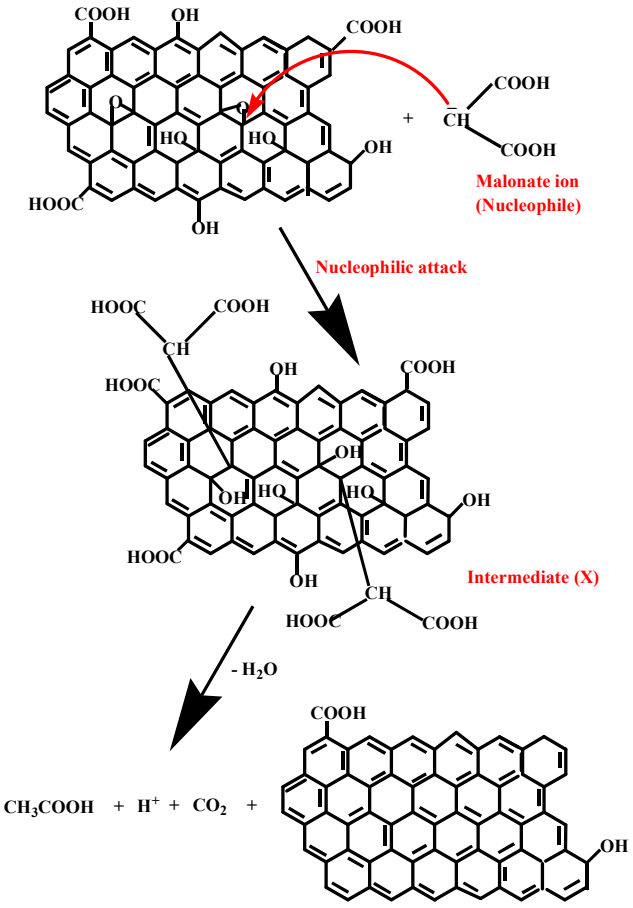

Scheme 1 Scheme depicting the nucleophilic attack of malonate ion on the epoxy group of GO resulting in the formation of graphene.

Further, the value of conductivity of GRH-MA is about two orders of magnitudes higher to that of GRH-Ox (1.03 x 10^{-2} S cm^{-1}) (Fig. S9, ESI†). Interestingly, the conductivity observed for GRH-MA is not only higher to that of similar reducing agent like oxalic acid investigated in the present work, but also of the same magnitude to those of other effective reducing agents reported earlier like $NaBH_4$[38] and L-ascorbic acid.[39]

The effectiveness of reduction by malonic acid at pH 10.5 is further revealed by the AFM data in which the thickness of GRH-MA was observed to be 0.41 ± 0.03 nm, which is slightly higher to that of the single layer graphene (0.34 nm) corresponding to the spacing between the two adjacent layers of graphite (Fig. 5). In view of the thickness of GO sheet of 1.23 nm estimated in the present work, it is apparent that the functionalities of GO has been reduced to a large extent by malonic acid reduction at this pH. A little higher thickness of graphene sheet as compared to that of the single layer graphene has possibly arisen due to the small amount of oxygen functionalities present on the reduced GO. On the contrary, the thickness of GRH-Ox was found to be 0.75 nm (Fig. S8, ESI†) which is significantly higher to that of GRH-MA (0.41± 0.03 nm). Thereby, suggesting the effectiveness of malonic acid in producing ultrathin graphene sheet due to the

involvement of active methylene group.

Annealing of the GRH-MA under mild thermal conditions (GRH-MA300) induces the transformation of amorphous graphene into crystalline exhibiting hexagonal structure with six fold symmetry. The observed difference in the intensity of spots in SAED pattern indicates the presence of monolayer in the annealed sample (Fig. 7c, Inset).[35] The lattice fringes in HRTEM image with an average 'd' spacing of 0.35 ± 0.01 nm suggests the production of more ordered structure of graphene upon annealing (Fig. 7c‴). This was also evidenced by XRD data, where the peak due to (002) plane became relatively less broad (Fig. 4). For this sample a reduction in the intensity due to –OH and –C-O groups in IR analysis suggests the increased removal of remaining oxygen functionalities (Fig. 8, curve c). It is also evidenced by a significant increase in the conductivity of GRH-MA300 (Fig. 11), suggesting the increased restoration of carbon network upon annealing. These observations are also reflected by TGA experiments, which showed much higher thermal stability for GRH-MA300 as compared to that of GRH-MA (Fig. 10).

As regards to the charge storing capacity of GRH-MA the CV measurements exhibit the C_s value of 173 F/g at 100 mV/s, which is about 1.35 times higher to that of GRH-Ox (128 F/g) and more than 23 fold higher to that of GO (7.5 F/g) (Fig. 12D). Further, a comparison of C_s value for GRH-MA at a scan rate of 100 mV/s with other chemically reduced graphene(s) and even for some of the N doped systems shows it to be much higher (Table S2, ESI†). It evidently indicates it to be an efficient supercapacitor. This behavior is also revealed by the GCD measurements in which the C_s value at a current density of 1.0 A/g was observed to be 254 F/g, which is 1.25 times higher to that of GRH-Ox (202 F/g) and an order of magnitude higher than that of GO (18.6 F/g), respectively under similar conditions of experiment (Fig. 12G). It may be mentioned that the value of C_s for GRH-MA is much higher as compared to those measured earlier for chemically reduced graphene as well as for some of the N doped systems (Table S2, ESI†). A long cyclic life and its stability are crucial for the practical applications of supercapacitor. Interestingly, no change in the C_s value (171 F/g) for the first 50 cycles followed by a slight increase to 177 F/g up to 200 cycles and, thereafter, virtually no change up to 1000th cycle (Fig. 12H and 12H- inset) suggest the fairly high cycling stability of as synthesized GRH-MA. These findings suggest the superior electrochemical properties of GRH-MA and its immense potential for efficient energy storage material.

Conclusions

In summary, we have successfully synthesized ultrathin graphene sheets using malonic acid as a reducing agent. The presence of active methylene group in malonic acid makes it an effective nucleophile, which results in its enhanced reducing capability as compared to those of dibasic acids. IR, Raman and XPS studies indicate the increased graphitic character in reduced GO. These investigations are also supported by the significantly higher conductivity of GRH-MA as compared to those of GO and even GRH-Ox, respectively. The crystallinity in GRH-MA could be induced under mild thermal conditions of annealing for GRH-MA300 as was revealed by its XRD, Raman and HRTEM investigation. This sample exhibited increased restoration of sp^2 character and four fold higher conductivity to that of GRH-MA. The observation of rectangular shape cyclic voltammogram for GRH-MA covering large area for the same amount of material as compared to GO clearly demonstrate it to be a good capacitor with EDLC behaviour. The symmetrical triangular shape in GCD measurements with high value of C_s at a high current density of 10 A/g suggests it to be an excellent storage material. Moreover, the repeating charge- discharge measurement withstanding 1000 cycles clearly illustrates its immense potential for energy storage applications.

Acknowledgments

Mahima Khandelwal is thankful to MHRD, New Delhi for the award of SRF and to Prof. R. Nath, Department of physics, IIT Roorkee for supporting this work. Thanks are also due to Head, IIC, IITR, Roorkee for providing the facilities of AFM, TEM and FE-SEM. We would also like to acknowledge the help of Prof. B. Viswanathan, IIT Madras, Chennai for XPS measurements.

Notes

Department of Chemistry, Indian Institute of Technology Roorkee, Roorkee - 247667, India
Fax: +91 1332 273560; Tel: +91 1332 285799;
E-mail: anilkfcy@iitr.ac.in; akmshfcy@gmail.com

†Electronic Supplementary Information (ESI) available: See DOI: 10.1039/b000000x/

References

1. Y. Liu, X. Dong and P. Chen, *Chem. Soc. Rev.*, 2012, **41**, 2283.
2. F. Schwierz, *Nat. Nanotechnol.* , 2010, **5**, 487.
3. A. A. Baladin, *Nat. Mater*., 2011, **10**, 569.
4. C. Chen, S. Rosenblatt, K. I. Bolotin, W. Kalb, P. Kim, I. Kymissis, H. L. Stormer, T. F. Heinz and J. Hone, *Nat. Nanotechnol*., 2009, **4**, 861.
5. K. S. Kim, Y. Zhao, H. Jang, S. Y. Lee, J. M. Kim, K. S. Kim, J.-H. Ahn, P. Kim, J.-Y. Choi and B. H. Hong, *Nature*, 2009, **457**, 706.
6. T. Kulia, A. K. Mishra, P. Khanra, N. H. Kim and J. H. Lee, *Nanoscale*, 2013, **5**, 52.
7. Y. Zhang, L. Zhang and C. Zhou, *Accounts chem. Res.,* 2013, **46,** 2329.
8. Z. Bo, Y.Yang, J. Chen, K. Yu, J. Yan and K. Cen, *Nanoscale*, 2013, **5**, 5180.
9. S. Lizzit, R. Larciprete, P. Lacovig, M. Dalmiglio, F. Orlando, A. Baraldi, L. Gammelgaard, L. Barreto, M. Bianchi, E. Perkins and P. Hoffmann, *Nano Lett*., 2012, **12**, 4503.
10. K. S. Subrahmanyam, L. S. Panchakarla, A. Govindaraj and C. N. R. Rao., *J. Phys. Chem. C*., 2009, **113**, 4257.
11. C. K. Chua and M. Pumera, *Chem. Soc. Rev*., 2014, **43**, 291.
12. S. Stankovich, D.A. Dikin, R. D. Piner, K. M. Kohlhaas, A. Kleinhammes, Y. Jia, Y. Wu, S. T. Nguyen and R. S. Ruoff, *Carbon*, 2007**, 45**, 1558.
13. D. Li, M. B. Müller, S. Gilje, R. B. Kaner and G. G. Wallace, *Nat. Nanotechnol.*, 2008, **3**, 101.
14. V. C. Tung, M. J. Allen, Y. Yang and R. B. Kaner, *Nat. Nanotechnol.*, 2009, **4**, 25.
15. G. Wang, J. Yang, J. Park, X. Gou, B. Wang, H. Liu and J. Yao, *J. Phys. Chem. C*, 2008, **112**, 8192.
16. H.-J. Shin, K. K. Kim, A. Benayad, S.-M. Yoon, H. K. Park, I.-S. Jung, M. H. Jin, H.-K. Jeong, J. M. Kim, J.-Y. Choi and Y. H. Lee, *Adv. Funct. Mater.*, 2009, **19**, 1987.

17. A. Ambrosi, C. K. Chua, A. Bonanni and M. Pumera, *Chem. Mater.*, 2012, **24**, 2292.
18. Z. Lei, L. Lu and X. S. Zhao, *Energy Enviorn. Sci.*, 2012, **5**, 6391.
19. S. Pei, J. Zhao, J. Du, W. Ren and H.-M. Cheng, *Carbon*, 2010, **48**, 4466.
20. W. Chen, L. Yan and P. R. Bangal, *J. Phys. Chem. C*, 2010, **114**, 19885.
21. T. Zhou, F. Chen, K. Liu, H. Deng, Q. Zhang, J. Feng and Q. Fu, *Nanotechnology*, 2011, **22**, 045704.
22. P. Song, X. Zhang, M. Sun, X. Cui and Y. Lin, *RSC Adv*., 2012, **2**, 1168.
23. X. Teng, M. Yan and H. Bi, *Spectrochim. Acta Mol. Biomol. Spectros.*, 2014, **118**, 1020.
24. L. Zhang, G. Chen, M. N. Hedhili, H. Zhnag and P. Wang, *Nanoscale*, 2012, **4**, 7038.
25. T. Lin, J. Chen, H. Bi, D. Wan, F. Huang, X. Xie and M. Jiang, *J. Mater. Chem. A*, 2013, **1**, 500.
26. W. S. Hummers and R. E. Offeman, *J. Am. Chem. Soc*., 1958, **80**, 1339.
27. A. Kumar and M. Khandelwal, *New J. Chem.*, 2014, **38**, 3457.
28. P. Cui, J. Lee, E. Hwang and H. Lee, *Chem.Commun*., 2011, **47**, 12370.
29. S. H. Tamboli, B. S. Kim, G. Choi, H. Lee, D. Lee, U. M. Patil, J. Lim, S. B. Kulkarni, S. C. Jun and H. H. Cho, *J. Mater. Chem. A*, 2014, 2, 5077.
30. H. Liu, L. Zhang, Y. Guo, C. Cheng, L. Yang, L. Jiang, G. Yu, W. Hu, Y. Liu and D. Zhu, *J. Mater. Chem. C*, 2013, **1**, 3104.
31. P. Su, H.-L. Guo, L. Tian and S.-K. Ning, *Carbon*, 2012, **50**, 5351.
32. J. Zhang, H. Yang, G. Shen, P. Cheng, J. Zhang and S. Guo, *Chem. Commun*., 2010, 46, 1112.
33. R. S. Dey, S. Hajra, R. K. Sahu, R. Raj and M. K. Panigrahi, *Chem. Commun*., 2012, **48**, 1787.
34. C. Botas, P. Álvarez, C. Blanco, R. Santamaría, M. Granda, M. D. Gutiérrez, F. Rodríguez- Reinoso and R. Menéndez, *Carbon*, 2013, **52**, 476.
35. Y. Hernandez, V. Nicolosi, M. Lotya, F. M. Blighe, Z.Sun, S. De, I. T. McGovern, B. Holland, M. Byrne, Y. K. Gun'ko, J. J. Boland, P. Niraj, G. Duesberg, S. Krishnamurthy, R. Goodhue, J. Hutchison, V. Scardaci, A. C. Ferrari and J. N. Coleman, *Nat. Nanotechnol.*, 2008, 3, 563.
36. K. Haubner, J. Murawski, P. Olk, L. M. Eng, C. Ziegler, B. Adolphi and E. Jaehne, *Chem. Phys. Chem*., 2010, 11, 2131.
37. The details of this system will be published elsewhere.
38. H.-J. Shin, K. K. Kim, A. Benayad, S.-M. Yoon, H. K. Park, I.-S. Jung, M. H. Jin, H.-K. Jeong, J. M. Kim, J.-Y. Choi and Y. H. Lee, *Adv. Funct. Mater.*, 2009, **19**, 1987.
39. J. Gao, F. Liu, Y. Liu, N. Ma, Z. Wang and X. Zhang, *Chem. Mater.*, 2010, **22**, 2213.

Graphical Abstract

A novel synthesis of ultra thin graphene sheets for energy storage applications using malonic acid as a reducing agent

Anil Kumar and Mahima Khandelwal

Department of Chemistry, Indian Institute of Technology Roorkee, Roorkee - 247667, India
Fax: +91 1332 273560; Tel: +91 1332 285799; E-mail: anilkfcy@iitr.ac.in

The novel synthesis of ultrathin graphene sheets (0.41 ± 0.03 nm) with increased sp^2 character, high specific capacitance and charge- discharge capability demonstrates its energy storage applications.